Published in final edited form as:
Rev Sci Instrum. 2021 January 01; 92(1): 015114. doi:10.1063/5.0031191.

A modular testbed for mechanized spreading of powder layers for additive manufacturing

D. Oropeza[1], **R. Roberts**[1,2], **A.J. Hart**[1]

[1]Department of Mechanical Engineering, Massachusetts Institute of Technology, Cambridge, MA 02139 USA

[2]School of Engineering and Sciences, Tecnologico de Monterrey, 64849, Mexico

Abstract

Powder bed additive manufacturing (AM) processes, including binder jetting (BJAM) and powder bed fusion (PBF), can manufacture complex three-dimensional components from a variety of materials. A fundamental understanding of the spreading of thin powder layers is essential to develop robust process parameters for powder bed AM, and to assess the influence of powder feedstock characteristics on the subsequent process outcomes. Toward meeting these needs, this work presents the design, fabrication, and qualification of a testbed for modular, mechanized, multi-layer powder spreading. The testbed is designed to replicate the operating conditions of commercial AM equipment, yet features full control over motion parameters including the translation and rotation of a roller spreading tool, and precision motion of a feed piston and the build platform. The powder spreading mechanism is interchangeable and therefore can be customized, including the capability for dispensing of fine, cohesive powders using a vibrating hopper. Validation of the resolution and accuracy of the machine and its subsystems, as well as the spreading of exemplary layers from a range of powder sizes typical of BJAM and PBF processes, are described. The precision engineered testbed can therefore enable the optimization of powder spreading parameters for AM and correlation to build process parameters in future work, as well as exploration of spreading of specialized powders for AM and other techniques.

I. Introduction

Additive manufacturing (AM), referring broadly to techniques that build three-dimensional parts through digitally controlled layer-by-layer processing, offers the possibility of geometric part complexity, batch-to-batch flexibility, reduced time for prototyping and iteration, and reduced material waste. As such, AM has applications in aerospace, automotive, healthcare, consumer goods, construction, and other industries [1–7]. Powder

Corresponding Authors: D. Oropeza (dan.oropeza@gmail.com), A.J. Hart (ajhart@mit.edu).
Author Contributions: CRediT taxonomy
Daniel Oropeza: Conceptualization, Methodology, Software, Validation, Formal analysis, Investigation, Resources, Data curation, Writing – original draft preparation, Writing – review and editing, Visualization, Supervision, Project administration, Funding acquisition. **Ricardo Roberts-Ugrinovic:** Software, Validation. **A. John Hart:** Conceptualization, Methodology, Writing – reviewing and editing, Project administration, Funding acquisition.

AIP Publishing Data Sharing Policy
Data available on request from the authors.

bed-based additive manufacturing process, including binder jetting (BJAM) and powder bed fusion (PBF), are of particular interest and can build intricate components from polymers, metals and ceramics, using powder feedstocks [3,7–13].

BJAM uses inkjet printing technology to selectively bind powders in each layer of the build [3]. For BJAM, spreading of a thin layer of powder (on the order of 10s μm in thickness) is commonly performed using a roller [11]. The choice of a roller and tailoring of its surface characteristics (e.g., material, roughness) is particularly important when smaller powder sizes (e.g., 5–25 μm diameter for steel alloys) are used, as the spreading mechanism must overcome interparticle forces that overwhelm gravitational forces [11]. After the formation of the powder layer in BJAM, an inkjet printhead is rastered over the build area and a binding agent is selectively deposited; the binder adheres the powders locally and to the previous layer [3]. After all the layers have been deposited and bound, the object is extracted and post-processed to produce the final part, often including final curing of the binder. For metal and ceramic BJAM, additional post-processing includes debinding, sintering and/or infiltration with a secondary material to increase part density [3,9,11].

In PBF processes, which typically use powders in the 15–45 μm diameter range, commercial equipment typically uses a blade mechanism rather than a roller [3,14]. This is because larger powders experience less significant cohesive forces, and the compliance and localized forces exerted by the blade accommodate surface deviations in the component (e.g., due to thermal stresses) [15,16]. After the formation of the powder bed layer in PBF, an energy source (i.e., laser or electron beam) is used to locally melt the powder particles into the desired geometry – fusing the powder particles within the layer and to the previous layer [3]. Heat treatments for metal PBF components are common to relieve internal stresses induced by the thermal gradients imposed by the process but may not be required for plastic components fabricated via PBF [3,17,18].

Therefore, spreading of a thin layer of powder (Figure 1) is a critical step which must be optimized to ensure fabrication of quality components through BJAM and PBF. For BJAM, particularly of metals and ceramics, the green part must undergo sintering to produce the final component, analogous to conventional sintering practices in powder metallurgy, powder injection molding, and ceramic processing [3,19]. Thus, homogeneous density of the powder bed and green part are necessary for uniform shrinkage and densification [19–23]. Additionally for BJAM, a highly-packed powder bed can reduce the adverse effect of powder ejection that results from ballistic impact of the binder droplet with the powder surface, which can otherwise cause defects in the powder bed [24–26]. For PBF, the formation of a dense and uniform powder bed is critical to the fabrication of dense and homogenous final parts, since low packing density and variations in the powder bed will result in melt pool instabilities that create voids and undesired surface roughness [27]. Ultimately for both BJAM and PBF, part density will influence the material properties (e.g., mechanical, electrical, thermal, magnetic) [28–34]. Thus, careful understanding of the underlying processes that can produce porosity and control homogeneity must be explored to ensure the process, part, and property optimization.

Prior studies of powder spreading for AM have utilized both commercial and custom equipment [15,16,35–63]. Escano et al. utilized a custom single-layer blade recoating testbed coupled with in-situ high-energy x-ray imaging to explore the effect of particle size on spreading dynamics (e.g., dynamic repose angle, slope surface speed, slope surface roughness) [15]. Yee utilized a multi-layer powder spreading testbed with a blade mechanism to explore the variation of surface quality and particle size distribution due to spreading speed and amount of excess powder [48]. Snow et al. developed a single-layer blade spreading mechanism to correlate powder rheology experiments (e.g., angle of repose, flow funnel, apparent/tapped density) with avalanche angle (i.e., dynamic repose angle) [50]. Using a commercial BJAM machine (ExOne R2), Bai et al. studied the effects of particle size distribution on powder bed green density [55]. Ali et al. adapted a commercial PBF AM machine (EOS M290) with a blade spreading mechanism) to explore the variation of powder bed density and surface roughness across the build volume [62]. Tan Phuc et al. used a contact image sensor along with a custom-built mechanism to detect powder bed defects during powder spreading with a blade [63]. And, Myers et al. employed a commercial BJAM machine (ExOne Innovent+), having a roller spreading mechanism, to study the influences of layer height and spreading speed on powder bed density and surface roughness [43]. These studies have provided insights on the role of powder size, size distribution, and spreading mechanism motion on layer quality, density, and roughness. Powder spreadability and thus packing density are typically best for particle sizes (>10 μm) and those with spherical shape [42,44,48,49,54–56].

However, the advancement of powder bed AM and its industrialization requires transferrable knowledge, which in turn requires precision instrumentation to facilitate parametric studies of each process step. In the case of powder spreading, such instrumentation must achieve representative AM spreading parameters (e.g., spreading traverse speed, layer height, roller rotation), include characterization of the precision of machine motion, enable exploration of different spreading and dispensing mechanisms (e.g., blade vs. roller, piston fed vs. hopper), and attain multi-layer powder spreading in a repeatable manner. In roller-based spreading, reported roller translation speeds range from 5–130 mm/s, and reported rotation speeds are 250–350 RPM [35–42,54–55,57,58]. When a blade is used for spreading, blade speeds of up to 150 mm/s are typically reported [50–53]. Thus, any custom research equipment must be capable of replicating similar conditions, in order to be relevant to commercial applications of BJAM and PBF. Additionally, few studies consider compaction of the powder using a roller [47,49], yet theory suggests that small amounts of compaction force can significantly increase packing density of the powder bed [22,64,65]. Further, powder bed density measurement techniques often require movement of the sample to a measurement device thus potentially affecting the accuracy and repeatability of the density measurement [44,48,49,54,62,66].

Here, we present the design and fabrication of a precision powder spreading testbed suited to investigation of fundamentals and process variables that influence powder spreading in BJAM and PBF techniques. Our testbed is modular and enables multi-layer spreading experimentation, and therefore can facilitate correlation among powder flowability experiments (e.g., angle of repose, flow funnel), AM process parameters (e.g., spreading speed, layer height, spreading mechanism), and powder bed properties. Compared to

commercial AM equipment, the testbed allows for experimentation with smaller quantities of powder and fully programmed control of the spreading device, feed piston, and build platform. The testbed's functionality is demonstrated via spreading of exemplary layers of powder having size distributions typically used in BJAM and PBF.

II. Design and construction of powder spreading testbed

A. Overview of system and specifications

The powder spreading testbed fits on a tabletop (500 mm x 500 mm x 250 mm) and was designed according to the target specifications listed in Table 1. The testbed is suited for spreading of polymer, metal, or ceramic powders depending on the tool and experiment parameters chosen. Figure 2 shows the corresponding CAD model and fabricated powder spreading testbed. Exemplary images from a powder spreading experiment are show in Figure 2d (Multimedia View). The following are the major modules of the machine:

Powder supply platform: Powder is supplied using a vertical platform (travel distance of 20 mm), consisting of a motorized axis and a custom-machined pillar and piston.

Build platform: The build platform emulates the surface where the part would be built in an AM machine. The build platform of the spreading testbed has a removable build plate with integrated load cell. These are attached to a motorized (vertical) axis via a custom-machined pillar and piston. The build platform has a vertical travel distance of 20 mm, is capable of measuring loads up to 100 N, and the build (spreading) area is 60 mm x 60 mm.

Modular powder spreading mechanism: A custom-designed linear motion system is used to translate the powder spreading mechanism over the powder supply and build platforms. The spreading mechanism has mounting features that allow the interchange of different spreading tools (e.g., motorized roller, stiff blade, compliant blade) and the addition of a hopper dispensing system for fine powders.

Software: A custom LabView program controls all system operations and allows for specification of all process parameters.

B. Detailed description of powder spreading testbed

The powder spreading testbed consists of a modular spreading mechanism mounted on a linear motion system to provide translational motion for powder spreading and two vertical stages to serve as the powder supply and platform, shown in Figure 2. During operation, the powder is supplied by raising the supply platform and the spreading mechanism (e.g., roller, blade) is advanced to transfer and spread the powder over the second vertical stage (build platform). The build platform thus dictates the layer thickness, as well as moderates the level of compaction performed by the roller. For the powder spreading and build platform, control over the spreader geometry, spreading mechanism translation speed and rotation, compaction, and layer height are possible in our custom system.

1. Powder and build platforms—Each of the power and build platforms is driven by a vertical stage (Standa 8MVT100–25-1) which is capable of reported 5 μm resolution in full-

step, a travel range of 25 mm, and a maximum load of 8 kg. The vertical stages are controlled via a stepper motor controller (Standa 8SMC5-USB-B9–2). A custom machined piston attaches to each stage, and to a powder plate and removable build plate, respectively. The piston plate and build plate holder have a recessed portion where a piece of felt is attached to seal the gap between the pistons and machine wells to prevent powder from falling through the powder wells. A load cell (MeasureX MLD66, 100 N capacity, 0.1 N resolution) can be mounted underneath the build platform to record the load experienced by the build platform during powder spreading and compaction. The load range of 0–100 N was selected to monitor forces during forward-rotating powder compaction which can optionally be used to densify the powder layer after spreading [64,65]. The load cell data is recorded using a data acquisition system (National Instruments NI-9237).

2. **Linear motion system—**Each side of the linear motion system consists of a stepper motor (Anaheim Automation 13Y104S-LW8), a ballscrew for linear actuation (Thomson Linear RM1610Z2), a flexible shaft coupling (uxcell L30xD25mm 6.35×10mm), and a linear profile rail with roller bearing block (Thomson Linear 522P25A and 512P25A1) – the linear motion system is mounted in a parallel configuration. The two stepper motors are synchronously controlled using a motion controller (Synthetos tinyG). To enable adjustment of parallelism and vertical offset between the spreading mechanism, the machine platform and the build plate, the linear motion system is mounted to the testbed baseplate using micrometers (Newport BM30.10, 10.0 mm travel range, 409 N individual load capacity) and bolts fed through stacked Belleville disc springs (McMaster Carr 96445K503). The parallelism between the spreading mechanism and build plate is set using bubble levels and the vertical offset is set using a shim of known thickness (e.g., 100 μm).

3. **Modular powder spreading system—**The carriage for the linear motion system contains mounting features enabling the attachment of a spreading mechanism suited to be chosen for powder and experiment. As examples, CAD models of three mechanism designs – motorized roller, stiff blade, and compliant blade – are shown in Figure 3. The roller mechanism has been fabricated here using a 20 mm high-speed steel shaft. To hold the roller, the 20 mm shaft is mounted on tapered roller bearings (SKF 32004 X/Q, static load capacity of 27 kN) and attached to a DC motor (Pololu 37D Gearmotor with Encoder) using a flexible shaft coupling (uxcell L30xD25mm 6×12mm). The DC motor is controlled via a motor controller (Pololu Jrk G2 18v19 USB) and the optical encoder integrated to the DC motor is read using a microcontroller (Arduino Nano).

4. **Powder hopper dispenser—**To facilitate mechanized metering of powder onto the build platform ahead of the spreading mechanism, a vibratory powder dispenser was developed. Direct, metered dispensing is desirable when spreading fine, cohesive powders, and as such the mechanism is integrated with the roller apparatus in the testbed. A CAD model of the dispensing system and picture of integration into the testbed are shown in Figure 4. The hopper consists of a custom machined aluminum funnel and sieve cover located at the base of the funnel, stainless steel wire cloth with 100 × 100 mesh size (McMaster Carr 85385T101), a turbine vibrator (McMaster Carr 3987K69), damping bolt attachments (McMaster Carr 93945K31), and a pressure regulator for the turbine vibrator.

The vibration frequency and force of the turbine vibrator is set by the backpressure supplied through the pressure regulator and cycled on/off using a microcontroller (Arduino Nano), a power relay, and an electric solenoid valve. The powder hopper system can be utilized in replacement of the piston feed system for supplying powder to the spreading mechanism, or in conjunction with the piston feed system to supply a secondary powder (i.e., material, size, shape) for additional exploration.

5. **Powder containment system—**A powder catch has been fabricated from machined aluminum, polymer via stereolithography, and compressive felt to fit at the end of the testbed's top plate to capture excess powder during the powder spreading process – shown in Figures 2a and 2b. To prevent powder contamination of the linear motion system, a thin plastic curtain (visible in Figure 2b) attached to retracting spring loaded tubes mounted to the machine baseplate separates the linear motion system from powder zone (i.e., powder supply, build platform, excess powder catch), thus preventing fouling of guides and ballscrews.

6. **Control and software architecture—**A custom LabView program was developed to enable integrated control of the testbed, and to allow automated repetition of layer spreading. Figure 5 schematically shows the electrical wiring and communications within the system. To provide inputs to the LabView program, a MATLAB script was developed to convert user inputs (e.g., desired layer height, spreader traverse speed, roller RPM, etc.) to a text file which contains LabView-compatible machine commands. The text file is then used as an input to the LabView code which uses the control commands to drive the machine.

III. Validation and analysis of the powder spreading testbed

A. Powder spreading testbed validation

To validate the motion system for the powder spreading testbed, the spreading traverse speed, vertical stage resolution, vertical stage stiffness, roller revolution, and roller runout were measured.

1. **Linear motion system: traverse speed—**The traverse speed of the linear motion system was measured using an optical encoder (US Digital EM-2) and linear encoder strip with 2000 LPI resolution (US Digital LIN 2000 LPI). The system was given commands to traverse forward and backward at speeds between 1.67 mm/s and 100 mm/s, with two measurements performed for each condition (i.e., speed and direction). Linear correlation was demonstrated within ±0.5 mm/s for the range of 0–100 mm/s for set and measured speeds using the encoder, as shown in Figure 6.

2. **Build platform: vertical stage resolution and stiffness—**The motion resolution of the build platform's vertical stage was measured using a dial indicator (Mitutoyo 543–791B Absolute Digimatic Indicator, resolution 0.001 mm, accuracy of 0.006 mm). The vertical stage was given commands to traverse up and down at increments ranging between 25 and 400 μm, with three measurements performed for each condition (i.e., position and direction). Linear correlation was demonstrated within ±2 μm for the range of −400 to 400

μm for set and measured vertical positions using the dial indicator, as shown in Figure 7a and 7b.

The stiffness of the vertical stage was measured using a dial indicator and a force gauge (Nextech DFS100, maximum 100 N, resolution 0.01 N). The measurements were performed by applying a force and measuring the deflection of the dial indicator. The stiffness was calculated from a linear fit of the force vs. displacement data, shown in Figure 7c, indicating a stiffness of 4.76 N/μm for the vertical stage. For estimated vertical forces during powder spreading of <100 mN [67], the expected deflection of the vertical stage due to powder spreading would be <0.1 μm.

Additionally, the load cell mounted under the build platform was calibrated using a set of precision weights and the native LabView Load Cell Calibration wizard. The calibration was performed with felt material placed within the powder well, reflecting the configuration intended for use during powder spreading experiments.

3. Roller powder spreading mechanism: roller revolution and runout—The rotational speed of the roller was measured using a non-contact tachometer (Checkline CDT-1000HD), with the DC motor at a gear ratio of 30:1 (Pololu 37D Metal Gear Motor with Encoder). RPM measurements were taken while providing the DC motor with speeds −330 to 330 RPM, with three measurements performed for each condition (i.e., RPM setting and direction). Linear correlation was demonstrated within ±1 RPM for the range of −330 to 330 RPM for set and measured rotational speeds using the tachometer, as shown in Figure 8.

The roller runout was characterized using a high-speed 2D laser profiler (Keyence LJ-V7060) by taking linear scans of a 40 mm section of the roller (parallel to its rotation axis) as the roller was rotated, thus providing a three-dimensional rendering of the roller shape. The runout measured over the 40 mm section was 30 μm, and for the central 10 mm region of the roller, the runout was 15 μm, as shown in Figure 9. The total runout is comparable to the average particle sizes typical for BJAM and PBF, yet importantly less than the typical thickness of a powder layer which is, to give uniform spreading, recommended as 3–5 times the mean particle diameter [68]. Also, additional energy is transferred to the powder particles from frictional shear between the powder and the roller, enhancing local layer uniformity. As such, it is important for the rotational speed to create a contact velocity between the roller and particle that is greater than the lateral traverse speed of the spreading mechanism. As an example, for a roller of 20 mm diameter, rotation at 250 RPM results in a surface speed of 262 mm/s which is greater than the common range of 1–20 mm/s for roller spreading mechanisms [58].

4. Hopper powder dispensing system: powder flow rate—The amount of powder dispensed from the hopper depends on the supplied pressure to the turbine vibrator and the length of time the hopper is vibrated. To develop an estimate of the powder flow rate from the hopper, the hopper was activated for pressures ranging from 20–60 psi and hold times between 0.5 and 20 seconds. Fine stainless steel 17–4 PH powder (<22 μm, Carpenter) was dispensed into on a weighing boat and weighed using a laboratory scale (Ohaus Corporation DV215CD, 0.01 mg resolution) after each experimental condition. Tests were completed

three times for each condition and were performed at 55.5% humidity (AcuRite 01080M), in an ambient lab environment. Figure 10a shows the correlation between pressure, time, and deposited mass – with deposited mass increasing with deposition time and backpressure. Figure 10b shows the dispensing rate for each pressure condition estimated from a linear fit of each dataset. This data can be used to estimate the parameters required for powder deposition via the hopper: for the given 17-PH powder (bulk density of 7.81 g/cm^3), an approximated powder bed packing density of 50%, and a build area of 60 mm x 60 mm, the required mass of powder for a 50 μm and 100 μm layer are 703 mg and 1406 mg, respectively. Additionally, for a spreading traverse speed of 5 mm/s and 10 mm/s, the traverse time will be 12 seconds and 6 seconds, respectively. Thus, for a 100 μm layer and 10 mm/s traverse speed, a setpoint of approximately 22 psi should provide sufficient powder for recoating of the layer. However, since the build piston area (70 mm x 70 mm) is larger than then build area (60 mm x 60 mm), the width (75.6 mm, perpendicular to motion direction) of the dispensing slot in the hopper is larger than the width of the build piston, and the build platform has recessed mounting features (11 mm x 11 mm x 3.5 mm) at its corners the dispensed powder will not all be deposited on the build platform and thus these calculations should only be utilized as first-order estimates.

In summary, these validation experiments demonstrate that the powder spreading testbed will be capable of attaining spreader traverse speed of 0–100 ±0.5 mm/s, roller RPM of 0–330 ±1 RPM, and micron-scale vertical piston motion for layer height control.

B. Powder spreading experiments

To validate the utility of the testbed, exemplary spreading experiments are now presented. The purpose of the following experiments is to showcase the operational capabilities of the powder spreading testbed (i.e., achieve AM-process relevant powder spreading) and is not intended as a full description of possible characterization methods for powder spreading experiments (e.g., powder bed density, powder surface roughness) to be performed by the testbed in future work.

1. Effect of layer height on layer uniformity—To showcase the influence of layer height on powder layer formation, stainless steel 316L powder (15–45 μm, John Galt Steel) was spread at set layer heights of 50 and 100 μm. To assess the influence of layer height on uniformity, an imaging setup (Thorlabs CMOS Camera DCC3240M, Thorlabs Coaxial Zoom Lens MVL6X3Z, Extension Tube MVL05A, C-Mount Adapter MVLCMC) was placed over the build platform using a coaxial lighting setup, as shown in Figure 11c. Powder was spread at a traverse speed of 50 mm/s without roller rotation at 47.7% humidity (AcuRite 01080M), in an ambient lab environment. For the 50 μm layer height (Figure 11a), we see regions of brightness which are the result of light reflection from the build plate, the result of sparse powder spreading due to inadequate layer height for the given powder size. For the 100 μm layer height (Figure 11b), we do not see high brightness regions, but instead a uniform powder distribution over the imaged area. A close-up and enhanced brightness image of the 100 μm layer, Figure 11d, reveals the packing of individual powder particles that make up the layer.

2. **Effect of simulated defect on powder layer—**To showcase the capability of the system to capture anomalies that may occur during AM, a simulated defect was placed on the roller by attaching Kapton tape with thickness of 55 μm and width of 6.00 mm (measured using a Mitutoyo Digital Micrometer Series 293), see Figure 12c. Stainless steel powder (15–45 μm, John Galt Steel) was spread with a layer height of 100 μm, on top of a previously spread powder layer of 250 μm. Powder was spread at a traverse speed of 50 mm/s without roller rotation at 47.7% humidity (AcuRite 01080M), in an ambient lab environment. To assist in imaging the defect, two imaging conditions were used – coaxial light and lateral light directed at the zone of interest, shown in Figure 12. For a control spreading experiment performed without a simulated defect (Figure 12a) we see a uniform powder layer with no noticeable difference between the coaxial and lateral lighting conditions; a close-up image of the lateral lighting condition reveals individual particles. For the spreading experiment performed with the simulated defect (Figure 12b), a defect is visible in the lateral light condition but not in the coaxial condition. The width of the defect (measured using ImageJ) is 6.02 mm which agrees with the 6.00 mm width of the Kapton tape used as the simulated defect.

3. **Spreading of fine powders—**Finally, the spreading of small powder—as suited to BJAM—can be challenging due to interparticle friction and cohesion. To showcase the possibility of using the testbed to explore spreading methodologies for fine powders used AM, fine stainless steel 17–4 PH powder (<22 μm, Carpenter) was spread using the testbed in various configurations. First, spreading was attempted using the roller with a machine-set layer height of 100 μm and traverse speed of 5 mm/s: (1) without rotation; (2) with rotation of 250 RPM; and (3) with rotation of 250 RPM and simulated texture using Kapton tape strips at 90-degree intervals, shown in Figure 13c. Powder experiments were performed at 47.7% humidity (AcuRite 01080M), in an ambient lab environment. Optical images of the spread layers were taken under identical camera settings and coaxial lighting conditions, as seen in Figure 13. For the roller without rotation, Figure 13a, non-uniform powder spreading occurs over the build platform, with regions of peaks and valleys, as well as vacant regions. For the roller with rotation, Figure 13b, non-uniform powder spreading occurs again, with vacant regions and fewer perceptible peaks and valleys on for the formed layer. For the roller with rotation and the textured surface, Figure 13c, powder is spread over the whole build area without vacancies, but peaks and valleys are still visible after spreading.

To further improve the results, the fine powder was deposited using the vibratory hopper and subsequently spread using the roller with traverse speed of 10 mm/s and roller rotation of 250 RPM. The powder was deposited and spread with a layer height of 100 μm, on top of a previously deposited and spread powder layer of 1000 μm at 55.5% humidity (AcuRite 01080M) in an ambient lab environment; the spreading sequence is shown in Figure 14a (Multimedia View). To ensure sufficient powder was supplied by the hopper, the hopper dispensing parameters were 25 psi pressure for the 1000 μm layer and 23 psi pressure for the 100 μm layer, with a dispensing time of 10 seconds. Optical images of the final layer were taken under identical camera settings as the previous fine powder spreading experiments and coaxial lighting conditions. The fine powder spread after deposition from the hopper results in uniform powder spreading, as seen in Figure 14b. In this case, powder is spread uniformly

over the build area, with exception at the corners where powder dispensing does not fill the gaps for the build platform bolts), with limited peaks and valleys visible. Together, these results validate the testbed's capabilities for a variety of powder sizes, and show that combination of spreading parameters (e.g., spreading mechanism texture, roller RPM, traverse speed, powder dispensing mechanism) are critical for optimization of spreading of fine, cohesive powders.

IV. Conclusions

This paper has presented the design, fabrication, and validation of a modular powder spreading testbed suited to study process fundamentals and novel adaptations of powder-based AM processes. Testbed subsystems were validated using relevant measurement techniques and exemplary powder spreading experiments were performed to showcase full testbed functionality. The modular design of the testbed allows for interchangeability of spreading tools, and the adaptation of spreading conditions to address differing powder sizes, materials, and particle shapes. By coupling this testbed with appropriate powder bed density and surface roughness measurement techniques, future work utilizing this testbed will study in detail the influence of powder parameters (e.g., powder shape, powder size distribution, material) and spreading parameters (e.g., spreading method, layer height, traverse speed, roller RPM, compaction methodologies) on powder bed formation, enabling correlation with relevant build parameters for BJAM and PBF AM.

Supplementary Material

Refer to Web version on PubMed Central for supplementary material.

Acknowledgements

This work was supported by a NASA Space Technology Research Fellowship to D.O. Additional financial support for hardware and experiments was provided by a grant from Lockheed Martin Corporation, and a gift from Robert Bosch, LLC. We thank Ryan W. Penny and Adam G. Stevens for their input during the writing process.

References

[1]. Tofail SAM, Koumoulos EP, Bandyopadhyay A, Bose S, O'Donoghue L, and Charitidis C, Materials Today 21, 22 (2018).

[2]. Allison A and Scudamore R (Eds.), Additive Manufacturing: Strategic Research Agenda (AM Platform, 2014).

[3]. Gibson I, Rosen DW, and Stucker B, Additive Manufacturing Technologies: Rapid Prototyping to Direct Digital Manufacturing (Springer, 2010).

[4]. Paolini A, Kollmannsberger S, and Rank E, Additive Manufacturing 30, 100894 (2019).

[5]. Fores E and Boyer R, Additive Manufacturing for the Aerospace Industry (Elsevier, 2019).

[6]. Wohlers T, Campbell I, Diegel O, Huff R, and Kowen J, Wohlers Report 2020: 3D Printing and Additive Manufacturing Global State of the Industry (Wohlers Associates, 2020).

[7]. Shirazi SFS, Gharehkhani S, Mehrali M, Yarmand H, Metselaar HSC, Adib Kadri N, and Osman NAA, Science and Technology of Advanced Materials 16, 033502 (2015). [PubMed: 27877783]

[8]. Chen Z, Li Z, Li J, Liu C, Lao C, Fu Y, Liu C, Li Y, Wang P, and He Y, Journal of the European Ceramic Society 39, 661 (2019).

[9]. Du W, Ren X, Ma C, and Pei Z, in Proceedings of ASME 2017 International Mechanical Engineering Congress and Exposition (The American Society of Mechanical Engineers, 2017).

[10]. Herderick E, in Proceedings of MS&T 11 (Materials Science and Technology, 2011).

[11]. Mirzababei S and Pasebani S, Journal of Manufacturing and Materials Processing 3, 82 (2019).

[12]. Kruth JP, Levy G, Schindel R, Craeghs T, and Yasa E, in Proceedings of the 3rd International Conference on Polymers and Moulds Innovations (University of College Ghent, 2008).

[13]. Ligon SC, Liska R, Stampfl J, Gurr M, and Mulhaupt R, Chemical Reviews 117, 10212 (2017). [PubMed: 28756658]

[14]. Nagarajan B, Hu Z, Song X, Zhai W, and Wei J, Engineering 5, 702 (2019).

[15]. Escano LI, Parab ND, Xiong L, Guo Q, Zhao C, Fezzaa K, Everhart W, Sun T, and Chen L, Scientific Reports 8, 15079 (2018). [PubMed: 30305675]

[16]. Chen H, Wei Q, Zhang Y, Chen F, Shi Y, and Yan W, Acta Materialia 179, 158 (2019).

[17]. Leuders S, Thone M, Riemer A, Niendorf T, Troster T, Richard HA, and Maier HJ, International Journal of Fatigue 48, 300 (2013).

[18]. Gibson I and Shi D, Rapid Prototyping Journal 3, 129 (1997).

[19]. German RM, Sintering Theory and Practice (Wiley, 1996).

[20]. Zwiren A and Murphy TF, International Journal of Powder Metallurgy 54, 39 (2018).

[21]. German RM and Bose A, Injection Molding of Metals and Ceramics (Metal Powder Industries Federation, 1997).

[22]. German RM, Particle Packing Characteristics (Metal Powder Industries Federation, 1989).

[23]. German RM, International Journal of Powder Metallurgy 23, 237 (1987).

[24]. Parab ND, Barnes JE, Zhao C, Cunningham RW, Fezaa K, Rollett AD, and Sun T, Scientific Reports 9, 2499 (2019). [PubMed: 30792454]

[25]. Sachs E, Cima M, Cornie J, Brancazio D, Bredt J, Curodeau A, Fan T, Khanuja S, Lauder A, Lee J, Michaels S, Annals of CIRP 42, 257 (1993).

[26]. Fan T, Droplet-powder impact interaction in three dimensional printing (Massachusetts Institute of Technology, 1996).

[27]. Lee YS and Zhang W, in Proceedings of the 26th Annual International Solid Freeform Fabrication Symposium (SFF Symposium, 2015).

[28]. Oh IH, Nomura N, and Hanada S, Materials Transactions 43, 443 (2002).

[29]. Guden M, Celik E, Hizal A, Altindis M, and Cetiner S, Journal of Biomedical Materials Research – Part B Applied Biomaterials 85, 547 (2008).

[30]. Martos M, Cuevas FG, and Cintas J, Applied Physics A 92, 375 (2008).

[31]. Steinitz R, Journal of Applied Physics 20, 712 (1949).

[32]. Francl J and Kingery WD, Journal of the American Ceramic Society 37, 99 (1954).

[33]. Jiles DC, Owen CV, and Spitzig WA, Journal of Nondestructive Evaluation 6, 119 (1987).

[34]. Moyer KH, McDermott MJ, Topolski MJ, and Kearney DF, Powder Technology 30, 51 (1981).

[35]. Polozov I, Sufiarov V, and Shamshurin A, Materials Letters 243, 88 (2019).

[36]. Nastac M, Lucas R, and Klein A, in Proceedings of the 28th Annual International Solid Freeform Fabrication Symposium (SFF Symposium, 2017).

[37]. Mendoza Jimenez E, Ding D, Su L, Joshi AR, Singh A, Reeja-Jayan B, and Beuth J, Additive Manufacturing 30, 100864 (2019).

[38]. Mostafei A, Rodriguez De Vecchis P, Buckenmeyer MJ, Wasule SR, Brown BN, and Chmielus M, materials Science and Engineering: C 102, 276 (2019). [PubMed: 31147000]

[39]. Enneti RK and Prough KC, International Journal of Refractory and Hard Materials 84, 104991 (2019).

[40]. Cramer CL, Elliott AM, Kiggans JO, Haberl B, and Anderson DC, Materials & Design 180, 107956 (2019).

[41]. Parans Paranthaman M, Shafer CS, Elliott AM, Siddel DH, McGuire MA, Springfield RM, Martin J, Fredette R, and Ormerod J, JOM 68, 1978 (2016).

[42]. Mostafei A, Rodriguez De Vecchis P, Nettleship I, and Chmielus M, Materials & Design 162, 375 (2019).

[43]. Myers K, Paterson A, Iizuka T, and Klein A, in Proceedings of the 30th Annual International Solid Freeform Fabrication Symposium (SFF Symposium, 2019).

[44]. Budding A and Vanaker THJ, in Proceedings of the Seventeenth CIRP Conference on Electro Physical and Chemical Machining (CIRP, 2013).

[45]. Zocca A, Gomes CM, Muhler T, and Gunster J, Advances in Mechanical Engineering 6, 491581 (2014).

[46]. Baker PR, Three dimensional printing with fine metal powders (Massachusetts Institute of Technology, 1997).

[47]. Gregorski SJ, High green density metal parts by vibrational compaction of dry powder in three dimensional printing process (Massachusetts Institute of Technology, 1996).

[48]. Yee I, Powder Bed Surface Quality and Particle Size Distribution for Metal Additive Manufacturing and Comparison with Discrete Element Model (California Polytechnic State University, San Luis Obispo, 2018).

[49]. Cao S, Qui Y, F Wei X, and Zhang HH, Journal of Materials Processing Technology 220, 231 (2015).

[50]. Snow Z, Martukanitz R, and Joshi S, Additive Manufacturing 28, 78 (2019).

[51]. Chen H, Wei Q, Wen S, Li Z, and Shi Y, International Journal of Machine Tools and Manufacture 123, 146 (2017).

[52]. Fouda YM and Bayly AE, Granular Matter 22, 10 (2020).

[53]. Desai PS and Higgs CF III, Metals 9, 1176 (2019).

[54]. Elliott AM, Nandwana P, Siddel DH, and Compton B, in Proceedings of the 27th Annual International Solid Freeform Fabrication Symposium (SFF Symposium, 2016).

[55]. Bai Y, Wagner G, and Williams CB, Journal of Manufacturing Science and Engineering 139, 081019 (2017).

[56]. Ziaee M and Crane NB, Additive Manufacturing 28, 781 (2019).

[57]. Dhanushka Uduwage DS, Binder Jet Additive Manufacturing of Stainless Steel-Hydroxyapatite Bio-composite (Minnesota State University, Mankato 2015).

[58]. Mostafei A, Elliott AM, Barnes JE, Cramer C, Nandwana P, and Chmielus M, Progress in Materials Science, 100707 (in press).

[59]. Van den Eynde M, Verbelen L, and Van Puyvelde P, Powder Technology 286, 151 (2015).

[60]. Cordova L, Bor T, de Smit M, Campos M, and Tinga T, Additive Manufacturing 32, 101082 (2020).

[61]. Chen H, Chen Y, Liu Y, Wei Q, Shi Y, and Yan W, International Journal of Machine Tools and Manufacture 153, 103553 (2020).

[62]. Ali U, Mahmoodkhani Y, Imani Shahabad S, Esmaeilizadeh R, Liravi F, Sheydaeian E, Huang KY, Marzbanrad E, Vlasea M, and Toyserkani E, Materials & Design 155, 495 (2018).

[63]. Tan Phuc L and Seita M, Materials & Design 164, 107562 (2019).

[64]. Liu J and De Lo DP, Metallurgical and Materials Transactions A 32, 3117 (2001).

[65]. Fischmeister PHF, in Proceedings of the Institution of Mechanical Engineers (IMechE, 1982).

[66]. Rishmawi I, Salarian M, and Vlasea M, Additive Manufacturing 24, 508 (2018).

[67]. Parteli EJR and Poschel T, Powder Technology 288, 96 (2016).

[68]. Meier C, Weissbach R, Weinberg J, Wall WA, and Hart AJ, Journal of Materials Processing Technology 266, 484 (2019).

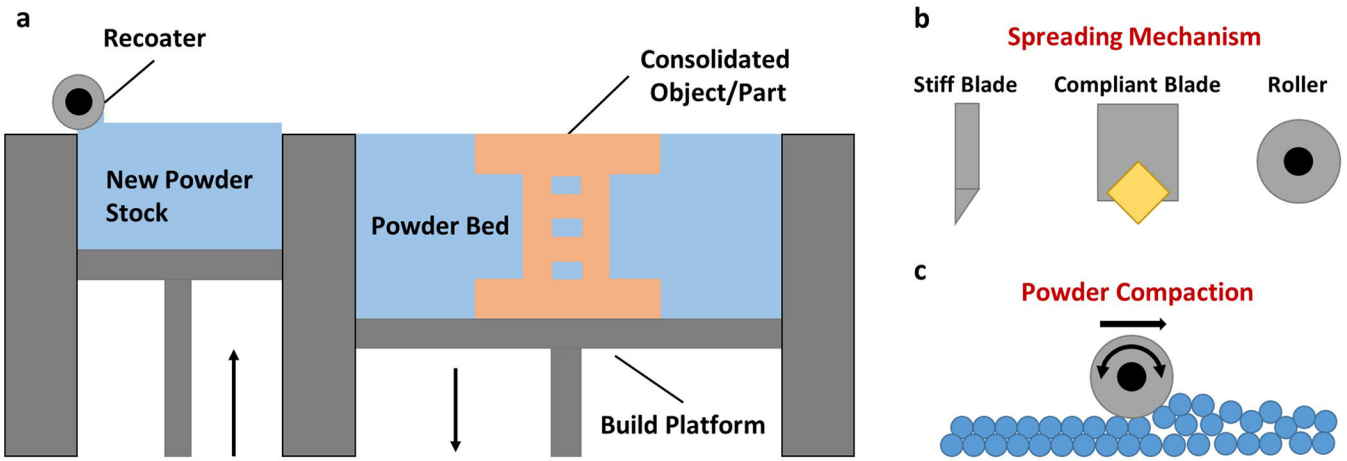

Figure 1 –.

Conceptual image of (a) powder spreading process for powder-based additive manufacturing, (b) powder spreading mechanisms, and (c) powder compaction during spreading process.

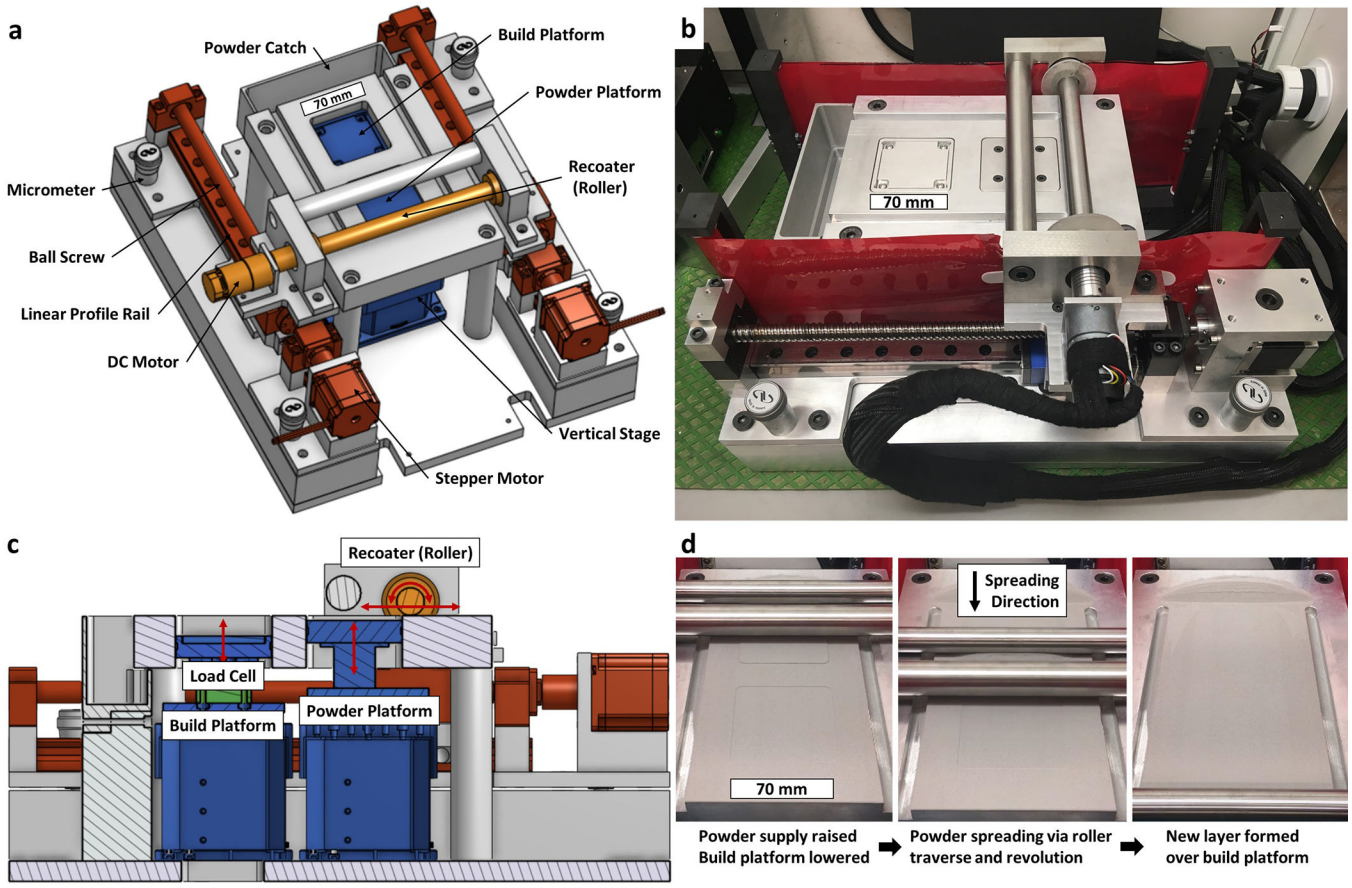

Figure 2 (Multimedia view) –.

Powder spreading testbed: (a) computer model showcasing major components with roller as powder spreading mechanism; (b) fabricated powder spreading testbed; (c) sectional side-view of testbed highlighting moving components and motion trajectories; (d) images from powder spreading experiment using stainless steel 316L 15–45 μm powder and 250 μm layer height.

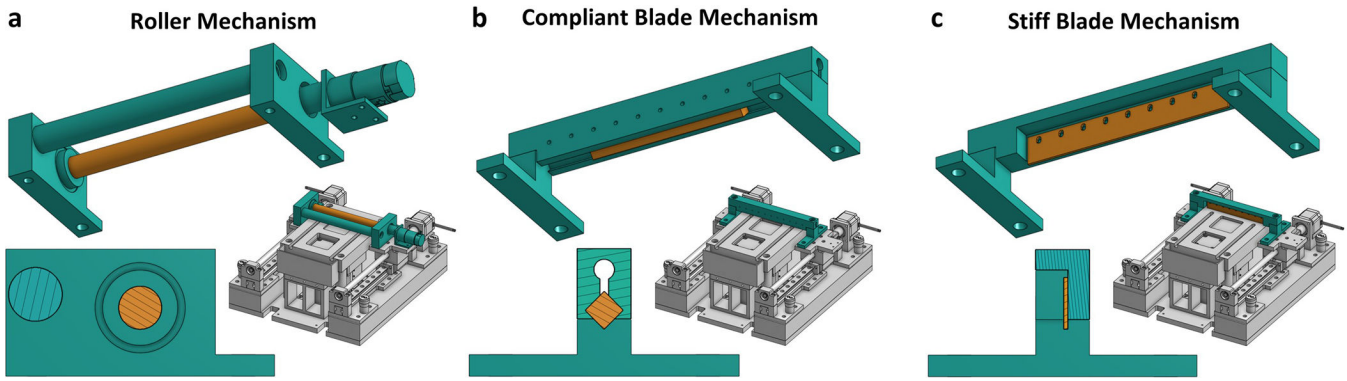

Figure 3 –.

Designs of various powder spreading mechanism configurations for testbed shown in assembled machine configuration, mechanism close-up, and side-view: (a) motorized roller, (b) compliant blade, (c) stiff blade.

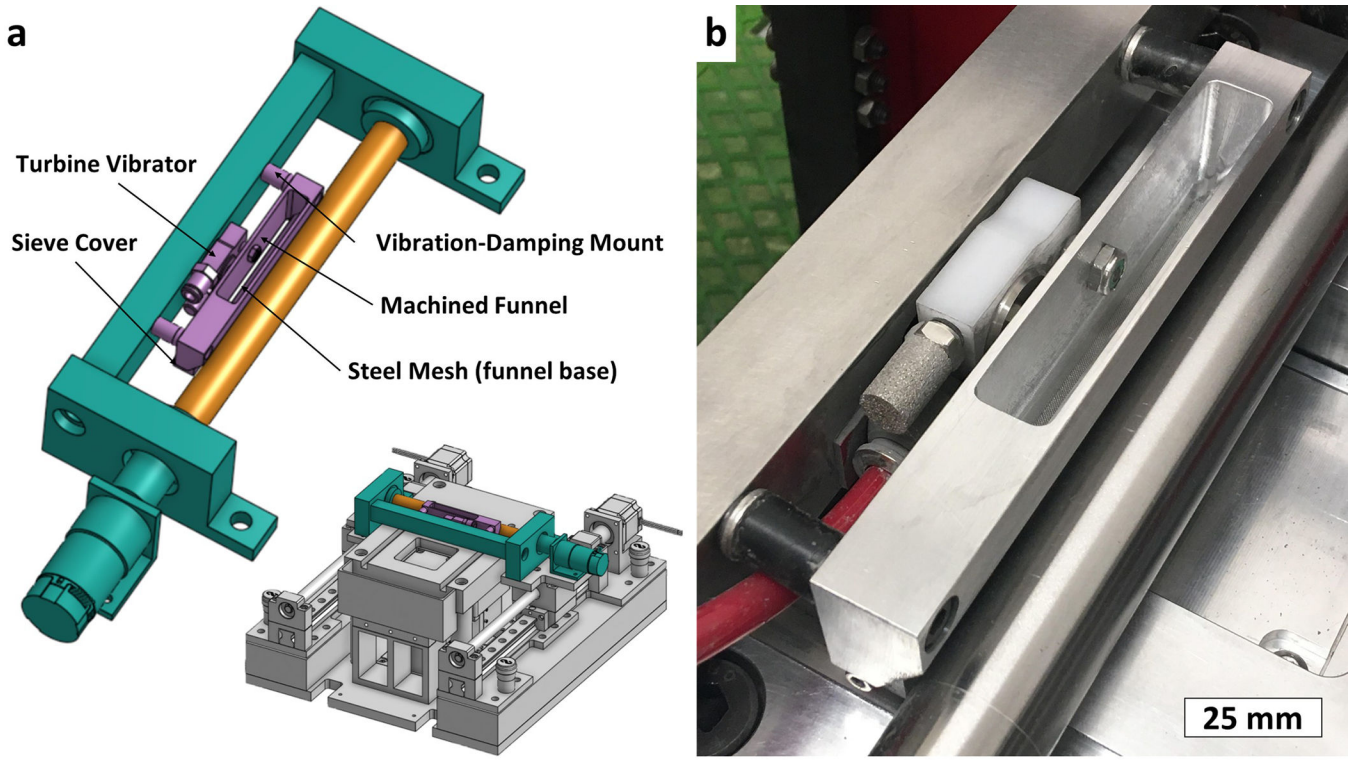

Figure 4 –.

Powder hopper dispensing system: (a) CAD design showing major components of hopper system and integration into testbed and (b) picture of hopper system mounted onto powder spreading testbed.

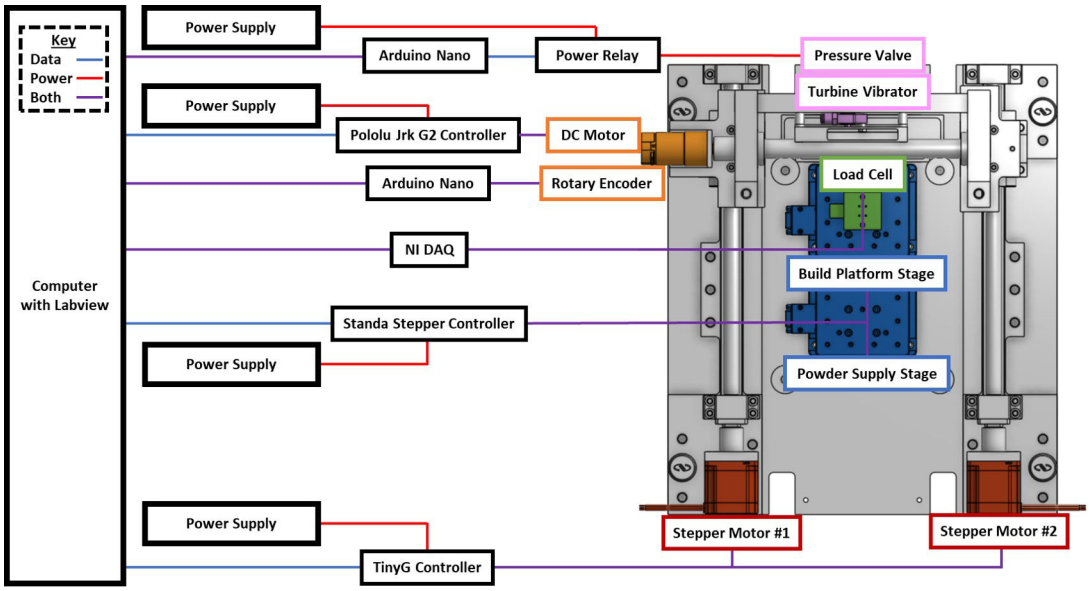

Figure 5 –.
Electronic connection diagram for powder spreading testbed.

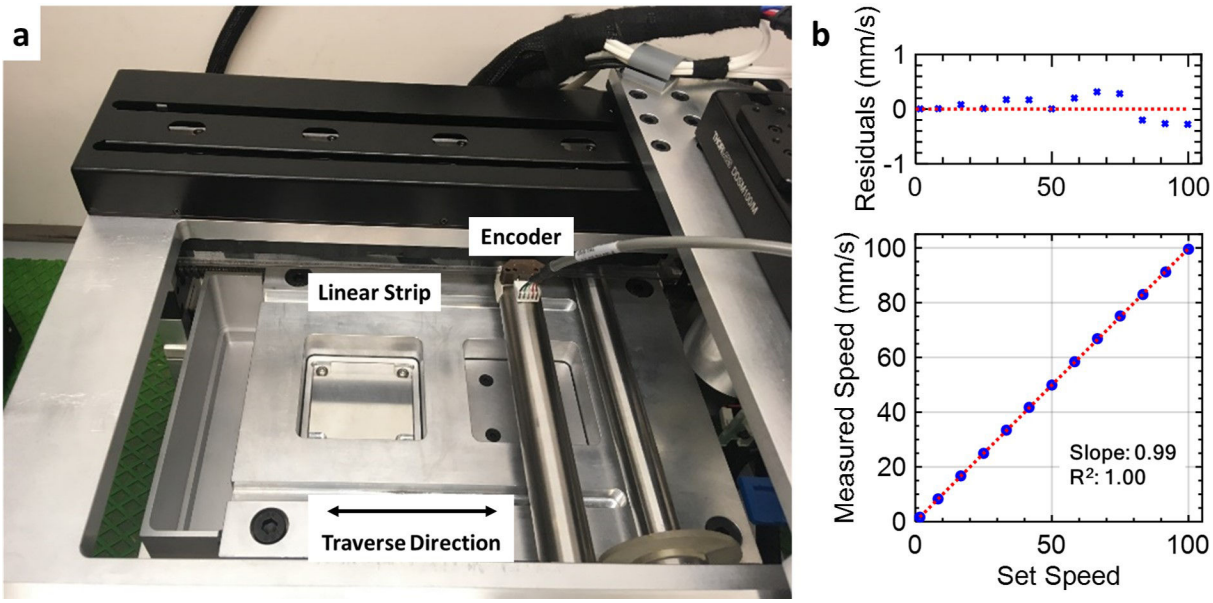

Figure 6 –.

(a) Validation test setup for spreading traverse speed and (b) plot of set versus measured speed with residuals to linear fit.

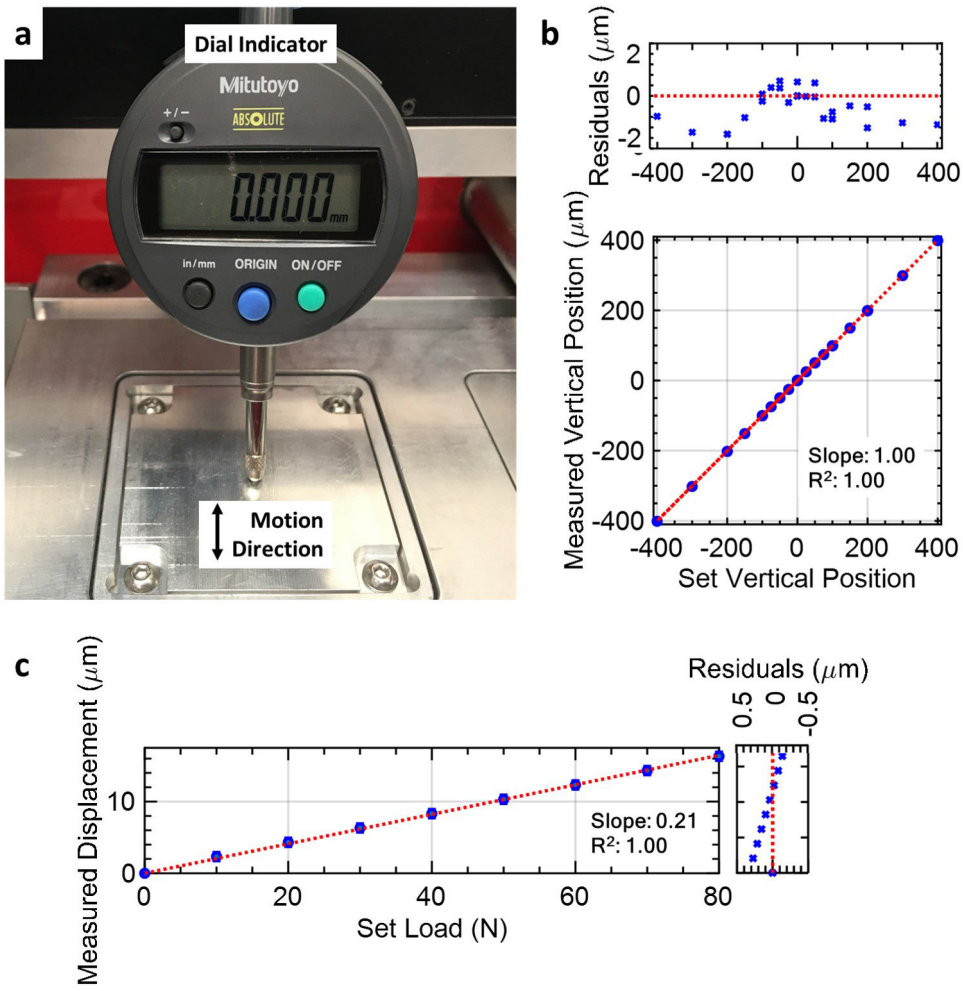

Figure 7 –.

(a) Validation test setup for vertical stage motion resolution, (b) plot of set versus measured position with residuals to linear fit, and (c) plot of set load versus measured displacement for build platform stiffness calculation with residuals to linear fit.

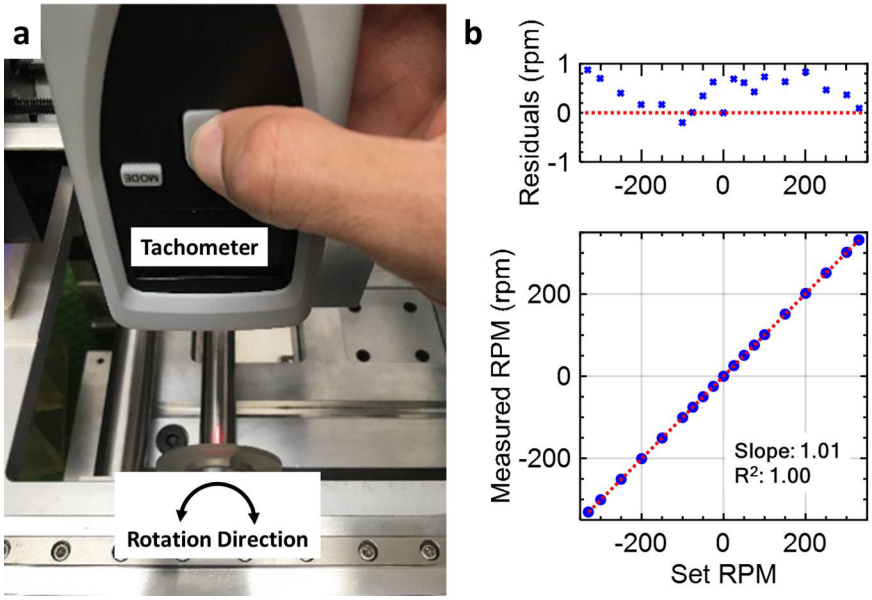

Figure 8 –.

(a) Validation test setup for roller RPM and (b) plot of set versus measured RPM with residuals to linear fit.

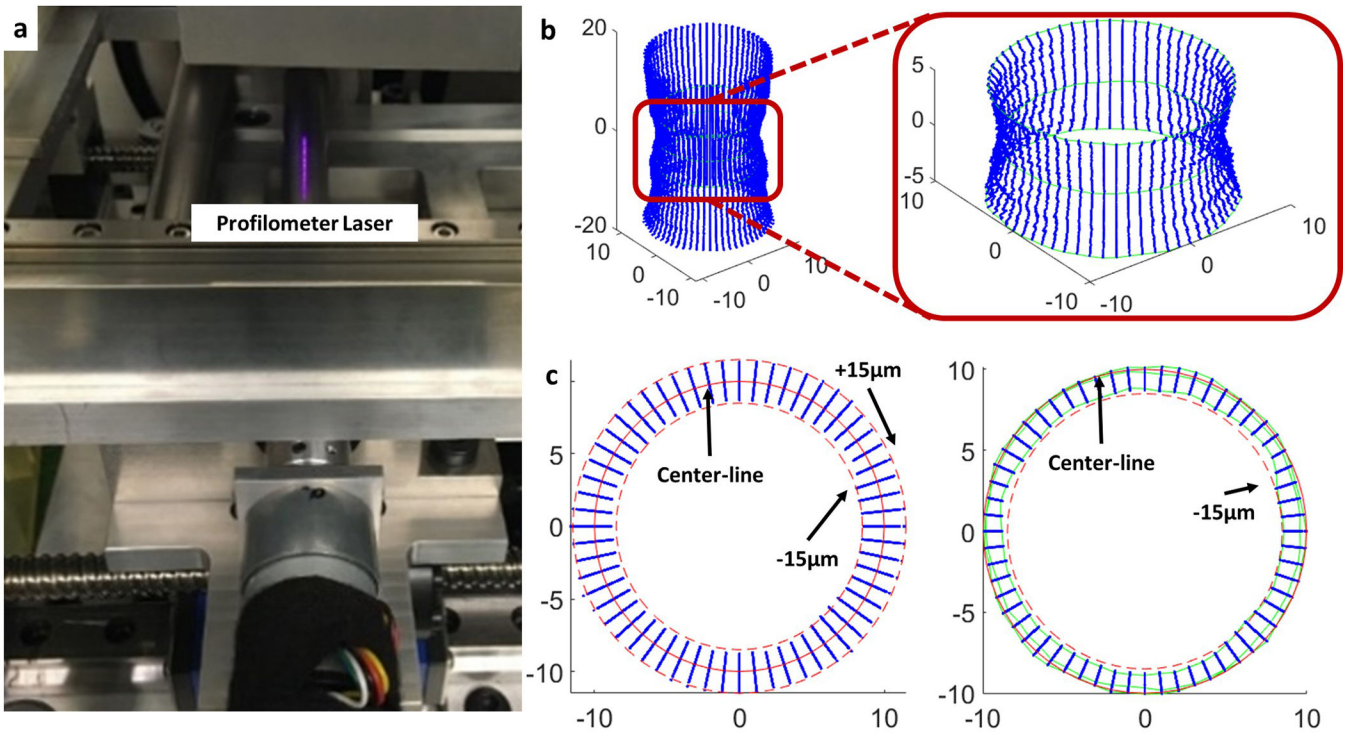

Figure 9 –.

(a) Validation test setup for roller runout and plots of runout versus position, (b) runout of roller for 40 mm measured section and 10 mm central section with runout values 100X for visualization, (c) runout plot for 40 mm measured section and 10 mm central section showing runout of 30 µm and 15 µm respectively. All axis units for runout figures (b, c) show position in mm.

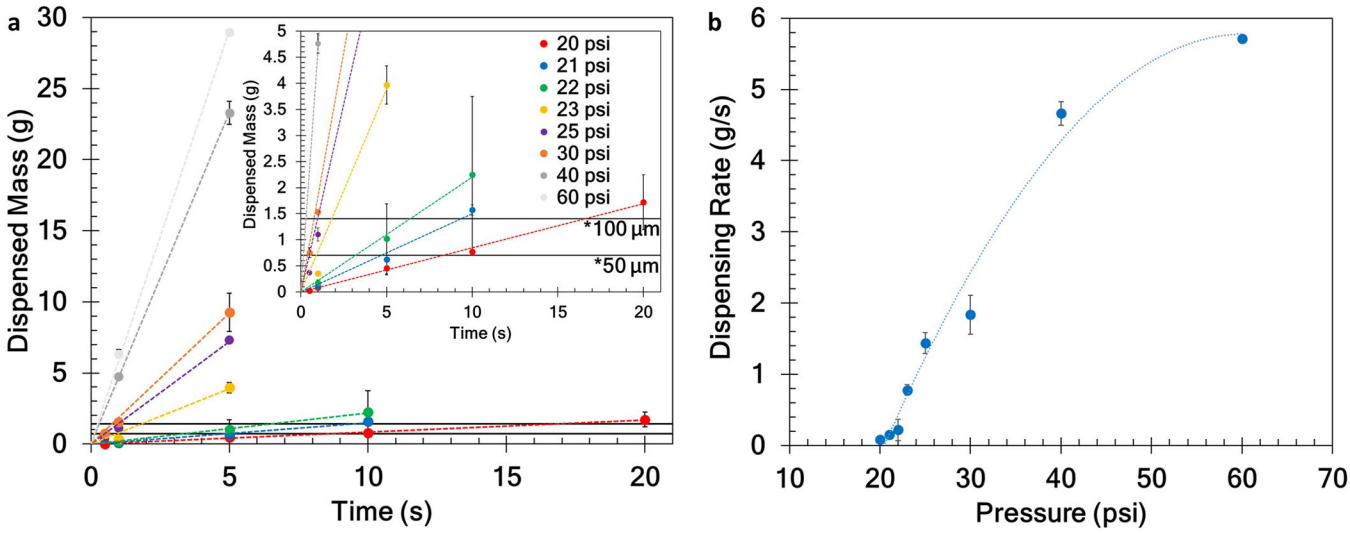

Figure 10 –.

Validation data from powder hopper dispensing experiment showcasing: (a) the relationship between backpressure to turbine vibrator, dispensing duration, and dispensed mass; and (b) the calculated dispensing rate at each pressure with quadratic fit.

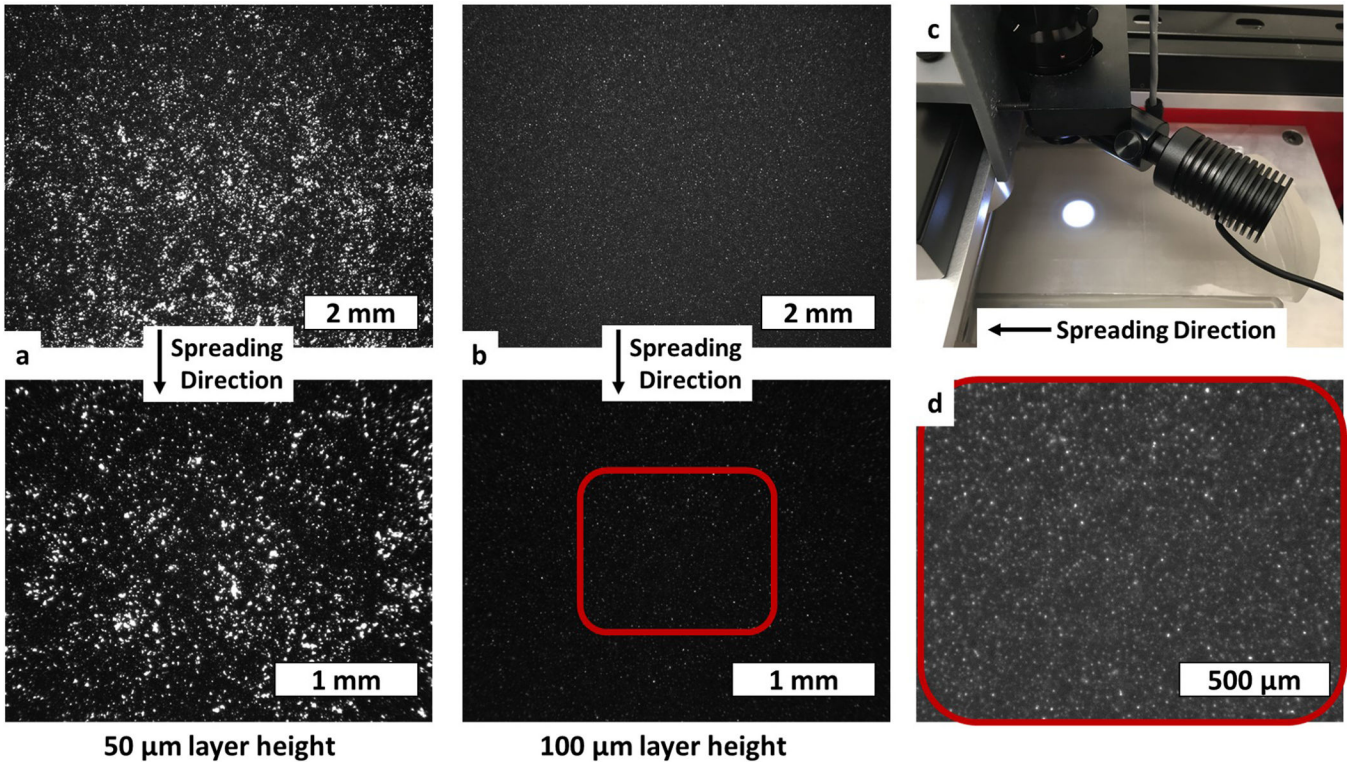

Figure 11 –.

Overhead images of powder layers of stainless steel 316L 15–45 µm powder at (a) 50 µm layer height and (b) 100 µm layer height showcasing difference in powder uniformity. Brightness in (a) is a result of light reflection from the baseplate and suggests an improperly spread powder layer. (c) Picture of testing condition and coaxial light setup. (d) Close-up and brightness enhanced image of 100 µm layer showing individual powder particles in layer.

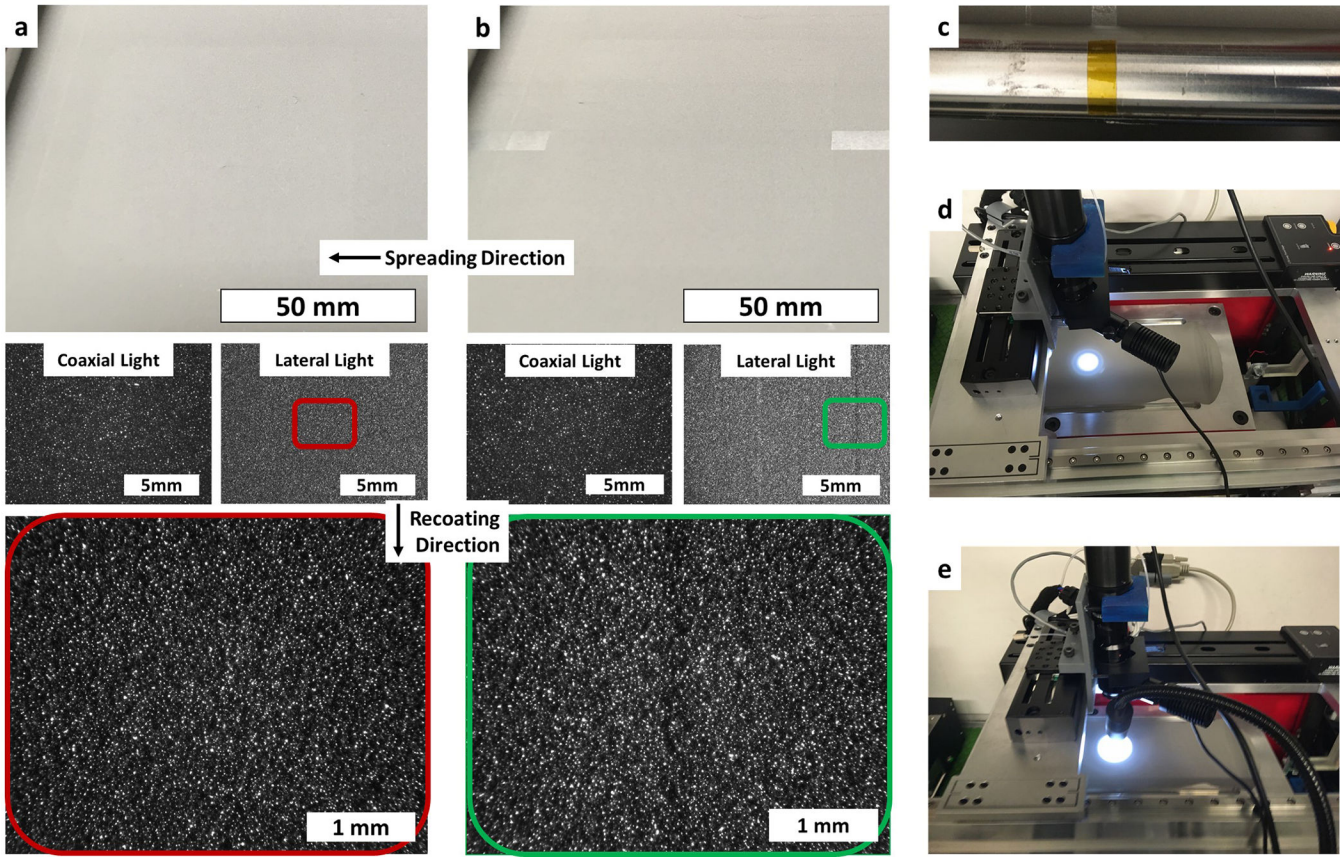

Figure 12 –.

Overhead images of powder layers of stainless steel 316L 15–45 μm powder using (a) no simulated defect and (b) simulated defect on the spreading mechanism. The lateral light imaging condition reveals the defect in (b). (c) Picture of simulated defect created by placing Kapton tape on the roller. (d) Picture of testing condition for coaxial lighting setup. (e) Picture of testing condition for lateral lighting setup.

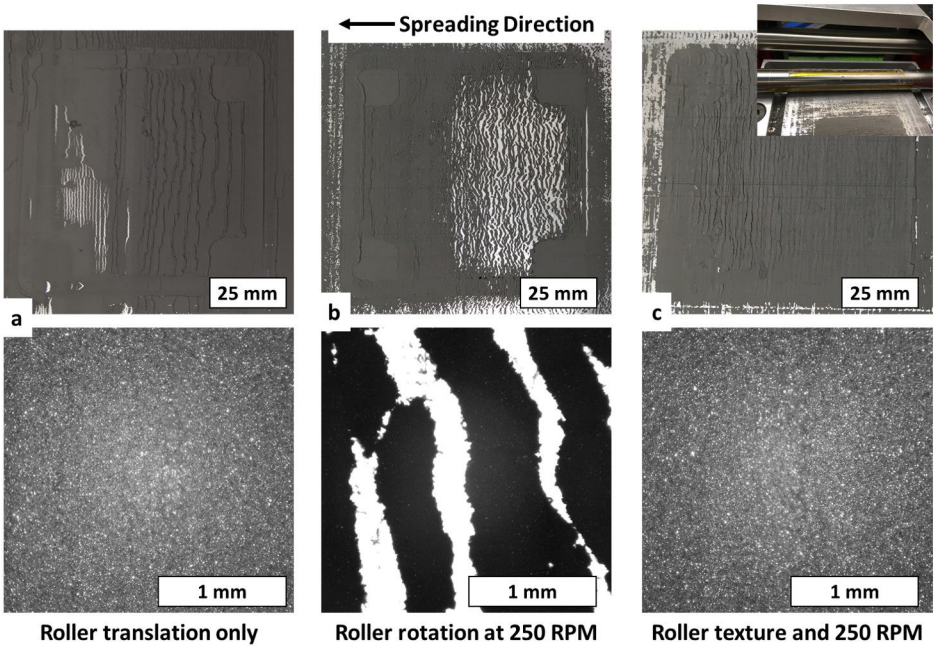

Figure 13 –.

Overhead images of powder layers of stainless steel 17–4 PH <22 μm powder using (a) no roller rotation, (b) roller rotation of 250 RPM and (c) roller rotation of 250 RPM and a simulated textured surface.

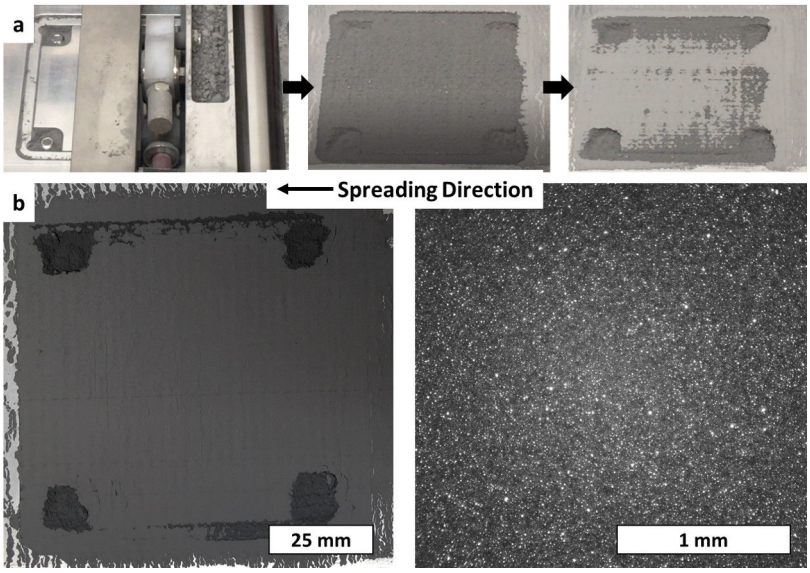

Figure 14 (Multimedia view) –.

Spreading of stainless steel 17–4 PH <22 μm powders using hopper dispensing and counter-rotating roller mechanism at 250 RPM: (a) showcasing deposition and spreading sequence of fine powders for base layer via hopper dispensing followed by roller spreading and (b) overhead images of final 50 μm thickness powder layer.

Table 1 –

Summary of desired design specifications for powder spreading testbed.

Parameter	Design Values
Spreading Tool Traverse Speed	0–100 mm/s
Roller Rotation	0–300 RPM
Build Platform Minimum Incremental Motion	5 μm
Powder Spreading Mechanism and Machine Platform Offset	0–1000 μm
Spreader Type	Modular; roller or blade
Powder Dispensing Mechanism	Modular; piston or hopper
Build Volume	60 × 60 × 20 mm
Machine Volume	480 × 415 × 250 mm